PHYSICAL REVIEW B VOLUME 28, NUMBER 12 15 DECEMBER 1983

Persistent nonphotochemical spectral hole dynamics for an infrared vibrational mode in alkali halide crystals

W. E. Moerner
IBM Research Laboratory, San Jose, California 95193

A. R. Chraplyvy
AT&T Bell Laboratories, Crawford Hill, Holmdel, New Jersey 07733

A. J. Sievers and R. H. Silsbee
Laboratory of Atomic and Solid State Physics, Cornell University, Ithaca, New York 14853
(Received 27 July 1983)

The dynamics of persistent nonphotochemical spectral-hole production in the ν_3 vibrational mode absorption of ReO_4^- molecules in alkali halide crystals are described and analyzed. The holes form at low temperatures with laser powers orders of magnitude below the saturation intensity I_s. The holes are shallow with steady-state widths and depths that are independent of burning laser power. As a function of burning time, the holes grow very slowly, with a near-logarithmic growth at short burning times and a less-than-logarithmic growth at long times. The holes may be erased using laser irradiation at frequencies near the hole frequency. A model is presented for this process in which reorientational tunneling between librational levels occurs during nonradiative vibrational decay. This photon-induced molecular reorientation model accounts for most of the observed properties. The observation of persistent spectral holes for a high-symmetry photostable molecule in an ordered, crystalline host shows that nonphotochemical hole burning is a general solid-state phenomenon that can be expected to occur whenever the complete ground state of a system has configurational degeneracy.

I. INTRODUCTION

Recently, the formation of persistent spectral holes by nonphotochemical or photophysical mechanisms has been reported for several inhomogeneously broadened optical transitions in solids.[1-3] A nonphotochemical mechanism is one in which the absorbing center does not itself undergo photochemical changes[4] (such as bond rearrangements, loss of ligands, etc.) during spectral hole formation. An important question to ask is the following: What are the basic requirements for the formation of nonphotochemical spectral holes that last much longer than excited-state lifetimes at low temperatures? In a general sense, the basic requirements for nonphotochemical hole formation are three. First, there must be several ground-state configurations of the total system, and the optical-absorption energies from these ground states must differ by more than the laser linewidth. Second, there must exist an optical pumping pathway that connects these ground-state configurations. Finally, the relaxation among the ground states must be slower than the excited-state lifetime. If all these conditions are met, persistent nonphotochemical holes can result.

Systems that have shown photophysical hole burning in the past have satisfied these requirements in various ways. For example, the electronic transitions of photostable molecules embedded in glasses[1] undergo persistent spectral hole burning due to interactions with the two-level systems characteristic of the glassy state. For the mixed molecular crystal pentacene in benzoic acid,[2] hole burning is thought to occur due to tautomerization of the hydrogen bonds in the dimer host lattice near the impurity. An infrared vibrational transition of 1,2-difluoroethane dispersed in amorphous Ar shows spectral hole burning,[3] presumably due to rearrangements of the nearby host matrix. For all of these cases, a rearrangement of the matrix near the impurity or a transition among some internal degrees of freedom of the matrix is responsible for the multiple ground-state configurations and subsequent formation of spectral holes.

In this paper we report the persistent spectral-hole dynamics for a high-symmetry photostable molecule in a simple, ordered crystalline host. The transition under study is the ν_3 internal vibrational mode of tetrahedral ReO_4^- molecules substitutionally doped into alkali halide single crystals. The holes were produced with 10.8-μm radiation from CO_2 and semiconductor diode lasers at intensities far below the two-level saturation intensity I_s. These holes have a variety of novel properties, and a thorough description of the hole dynamics and possible mechanisms forms the remainder of this paper. A preliminary report of this work has already appeared.[5]

The observation of spectral holes for ReO_4^- molecules in alkali halides proves that neither host rearrangement nor tautomerism is essential for the formation of persistent nonphotochemical holes. The hole formation in this system appears to involve reorientation of the excited impurity molecules during nonradiative vibrational de-

excitation. As a result of these measurements, persistent nonphotochemical hole burning at low laser intensity is shown to be a general solid-state phenomenon which may be reasonably expected to occur whenever the ground state of the system has configurational degeneracy.

II. EXPERIMENTAL

Two principal experimental arrangements were used for these experiments: one setup using two CO_2 lasers and a second setup employing a semiconductor diode laser and a CO_2 laser. Complete details of the experimental apparatus may be found in Ref. 6.

A. Hole burning with two CO_2 lasers

Figure 1 shows the experimental setup for CO_2-laser—CO_2-laser hole burning. A continuous-wave, longitudinally excited CO_2 laser was used as the vertically polarized tunable probe. Tunability was achieved by varying the cavity length with a piezoelectric transducer on the output mirror. No active cavity length or cavity temperature stabilization was used for these experiments. Since the laser was operated on low-gain, high-J lines, single longitudinal mode operation was easy to achieve, and the laser could be cavity-length tuned over roughly an 80-MHz range. Following the probe beam path in Fig. 1, the average power was monitored with a thermopile detector. A portion of the probe beam was split off and sent to a heterodyne beat detector to be described below. Calibrated CaF_2 attenuators at position A_B were used to adjust the probe intensity at the sample. The probe beam was chopped at 167 Hz (50% duty cycle). A 10-in.-focal-length ZnSe lens focused the probe beam on the sample, yielding a spot radius of 0.035 cm at the $1/e^2$ point. The sample was mounted in a variable temperature (1.2—300 K) optical cryostat with ZnSe inner and NaCl outer windows. The sample was usually oriented at 45° as shown in the figure, in order to minimize the scattered pump radiation at the detector. A 5-in.-focal-length ZnSe lens after

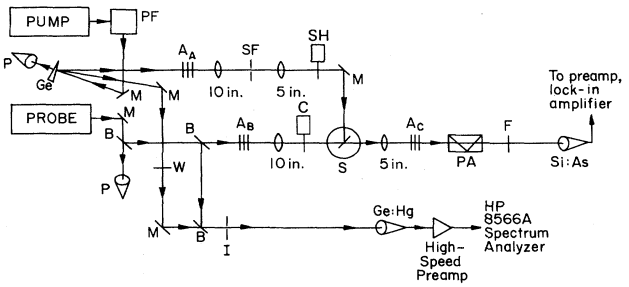

FIG. 1. Experimental arrangement for CO_2-laser—CO_2-laser hole-burning spectroscopy. Legend: A_A,A_B,A_C, CaF_2 attenuators; B, beam splitter; C, chopper; F, narrow-band filter (10.6—11.35 μm); Ge, uncoated Ge wedge (2°) beam splitter; Ge:Hg, photoconductive Ge:Hg detector; I, iris for alignment of heterodyne signal; M, mirror; P, power meter; PA, stack-of-plates polarization analyzer; PF, two-mirror polarization flipper; S, sample in variable-temperature cryostat; SF, 0.011-in. spatial filter; SH, shutter; Si:As, high sensitivity Si:As detector; W, zeroth-order $\lambda/2$ wave plate.

the cryostat recollimated the probe beam, and more CaF_2 attenuators at position A_C allowed the signal at the detector to be adjusted. A ZnSe stack-of-plates polarizer was used to reject horizontally polarized scattered pump radiation. Just before the detector, a narrow-band ir filter (10.6—11.3 μm) was used to reject black-body noise from the laser discharge. This filter was essential at low power levels because with 30 mm of CaF_2 in the probe beam, the broadband black-body signal from the laser discharge passing through the attenuators was larger than the 10.8-μm ir signal. Finally, an extremely sensitive liquid-He-cooled Si:As detector was used to measure the hole-burning signal corresponding to the sample transmission. The amplified signal from the detector was bandpass filtered (3 Hz—10 kHz) and analyzed with a lock-in amplifier. The lock-in amplifier output was normalized to the probe laser average power using a precision digital ratiometer, and the resulting voltage proportional to the sample transmission was recorded on an x-y recorder.

For a number of experiments, the probe laser was used to both burn and simultaneously detect the holes. However, for erasing experiments, a second CO_2 laser, called the pump, was required. The pump beam was generated by a second continuous-wave longitudinally excited CO_2 laser operating on the same laser line as the probe laser. The pump laser was cavity-length-tuned to adjust its oscillation frequency relative to the probe laser. Following the pump beam path in Fig. 1, the vertically polarized beam exiting from the laser was sent through a two-mirror polarization flipper to produce horizontally polarized radiation. Using a wedged Ge beam splitter, the beam was split into a sample beam and a beam for heterodyne frequency calibration. The polarization of the latter beam was rotated back to the vertical using a zeroth-order $\lambda/2$ wave plate. This beam was superposed in space with the vertically polarized beam from the probe and was sent to a Ge:Hg photoconductive heterodyne beat detector. Relative frequency calibration of the two lasers was achieved by observing the amplified heterodyne beat from the Ge:Hg photoconductive detector on a precision spectrum analyzer. The beat could be observed at frequency differences up to 40 MHz. The peak-to-peak jitter of the heterodyne beat was 2.5±0.5 MHz for a 3-sec averaging time. This frequency jitter resulted from discharge index of refraction and cavity-length fluctuations of the two lasers, and defined the frequency resolution limit of the experiment.

The pump beam used for erasing was attenuated by CaF_2 flats at position A_A and then was carefully spatially filtered through a 0.011-in.-diam pinhole in 0.005-in.-thick stainless-steel shim stock. This spatially filtered and attenuated pump beam was controlled by a manual shutter before impinging on the sample. The resulting beam at the sample was Gaussian in transverse distribution with a beam radius of 0.073 cm (at the $1/e^2$ point).

B. Diode-laser—CO_2-laser hole burning

Figure 2 shows the apparatus that was used for burning and detecting holes with a semiconductor diode laser and a CO_2 laser. For most experiments, holes were burned

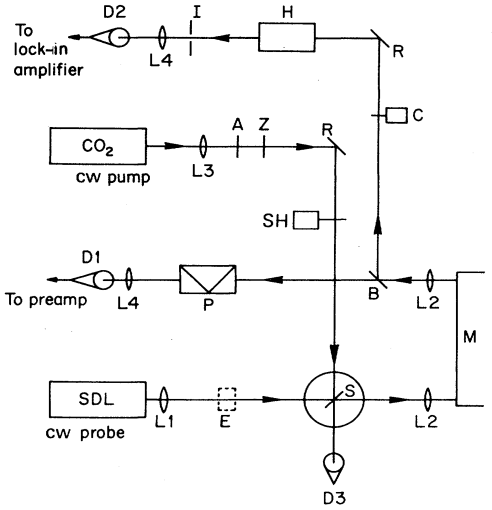

FIG. 2. Experimental arrangement for CO_2-laser—diode-laser hole-burning spectroscopy. Legend: *A*, CaF_2 variable attenuators; *B*, beam splitter; *C*, light chopper; *D*1, main HgCdTe detector; *D*2, hot CO_2 cell HgCdTe detector; *D*3, transmitted pump pulse detector; *E*, Ge étalon; *H*, hot CO_2 gas cell; *I*, iris; *L*1, 1.5-in. focal length antireflectance-coated collecting lens; *L*2, *f*-number matching lenses for monochromator; *L*3, pump focusing lens; *L*4, detector focusing lenses; *M*, 0.75-m monochromator; *P*, polarization analyzer; *R*, mirror; *S*, sample in variable-temperature helium Dewar; SH, shutter; *Z*, zero-order $\lambda/2$ wave plate; SDL, semiconductor diode laser.

with the CO_2 laser and detected with the diode laser. However, for some measurements, the holes were both produced and detected with the diode laser.

A longitudinally excited, continuous-wave CO_2 laser operating on the 10.8-μm *P*(42) line was used as a pump. The pump beam was focused on the sample in a variable-temperature optical cryostat with a 30-in.-focal-length ZnSe lens and was attenuated with calibrated CaF_2 flats. A zeroth-order wave plate was used to rotate the polarization of the pump laser into the horizontal plane. A low speed shutter was used to irradiate the sample with pump radiation for variable time periods. A pulse detector after the sample provided a reference trigger signal. The pump spot size at the sample was approximately 2.3 mm in diameter.

The probe beam was generated by a current- and temperature-tuned $Pb_{0.86}Sn_{0.14}Te$ semiconductor diode laser. The laser was maintained near 20 K in a closed-cycle helium refrigerator, and laser frequency jitter due to current and temperature fluctuations was 10 MHz. The diode laser was operated cw, and the laser control module was set to produce a sawtooth current waveform at roughly 500 Hz, which caused the laser frequency to scan over a range of about $\pm$125 MHz every 2 msec. A removable 2.54-cm Ge étalon was used to generate rough frequency calibration and verify single-mode operation.

After passage of the vertically polarized beam through the sample in a variable-temperature optical cryostat, a 0.75-m monochromator was used to reject unwanted longitudinal modes. The probe spot size at the sample was roughly 7 mm in diameter yielding an intensity of roughly 100 μW/cm^2. After passing through a vertically oriented polarizer, the main probe beam was detected with a 77-K HgCdTe detector, a narrow-band preamplifier (1 kHz—1 MHz), and a transient digitizer or a digital storage scope. The digitizer was triggered to acquire a single 2-msec scan of the probe laser at a variable delay from the start or end of the pump pulse. These time-delayed spectra were recorded and processed by a digital computer.

A considerable amount of effort was necessary in order to find the laser operating conditions that would generate tunable radiation including the *P*(42) CO_2 laser frequency, 922.9153 cm^{-1}. To accomplish this, part of the probe beam was split off, chopped, and sent through a hot cell containing 20 Torr of CO_2 at 300 °C before impinging on a 77-K HgCdTe detector. By interrupting the high-speed sawtooth scan of the laser and slowly ramping the laser current, the lock-in detected signal from this detector could be monitored for CO_2 absorption dips. In this manner, suitable dc current offsets and laser operating temperatures could be determined for operation near the CO_2-laser-line.

In order to provide frequency calibration of the time-delayed hole spectra, the CO_2-laser cavity length was adjusted to produce oscillation in two longitudinal modes. The spacing between the two holes thus burned (80$\pm$10 MHz) was measured relative to the Ge étalon fringe spacing of 0.049 18 cm^{-1}.

C. Alkali-halide crystals doped with ReO_4^- molecules

The samples used for these experiments were annealed, Czochralski-grown single crystals of KI or RbI. The crystals were doped by the addition of from 0.02 to 0.8 mol % of $KReO_4$ or $RbReO_4$ to the melt. The KI crystals were doubly doped with either 2.5 mol % Rb^+, 2.0 mol % Na^+, or 0.2 mol % Cs^+ ions in order to produce coincidences with the *P*(42) CO_2-laser line. The actual concentrations of the dopant ions in the grown crystals were somewhat smaller than these values due to partial evaporation of the dopant during the pulling process. The high-resolution linear spectroscopy of the ν_3 internal mode of ReO_4^- molecules in alkali halides has already been described.[7] Furthermore, *transient* hole-burning studies and incoherent laser saturation have already been used to measure T_1 and T_2 for the ν_3 excited state as a function of temperature and host crystal.[8] For all of the hole-burning studies reported in this paper, the holes are persistent (i.e., last much longer than T_1), and laser intensities were maintained orders of magnitude below the saturation intensity of $\sim$10 W/cm^2.

III. RESULTS

In this section, the results of a variety of experiments designed to elucidate the properties of persistent spectral holes in ReO_4^-—alkali-halide systems are presented. The CO_2-laser—diode-laser techniques described in Sec. II B are utilized whenever possible. However, the diode laser apparatus was only available for short periods of time. Consequently, many properties had to be studied with one or two CO_2 lasers only as in Sec. II A. The presentation

of results is organized by property measured rather than by experimental technique.

A. Lifetime, hole depth, and growth curves

Figure 3 shows the growth and detection of a persistent spectral hole in RbI:ReO_4^- using a single CO_2 laser (called the probe) as described in Sec. II A. The fixed-frequency probe laser burns a hole, and the time-varying probe laser transmission serves as a measure of hole depth. This technique has the virtues of simplicity and freedom from artifacts; however, the size of the hole is measured at line center only. After cooling a sample of RbI:ReO_4^- to 1.4 K in the dark, the laser is unblocked at time t_1 [Fig. 3(a)]. The vertical axis in Fig. 3 shows the infrared power transmitted through the sample as a function of time. Immediately after the laser unlocking, the sample transmission begins at the value T_i; it then slowly grows over many seconds to a steady-state value T_{ss}. After a dark period of 10 min the laser is again unblocked at time t_3 [Fig. 3(b)]: The sample transmission has remained at the larger value T_{ss}, indicating that the hole did not observably decay during this time interval. Longer dark times could not be studied due to drift of the CO_2-laser frequency during the dark interval.

Several conclusions may be drawn from data such as that presented in Fig. 3. First, the hole lifetime at 1.4 K is a good deal longer than 10 min. Second, the hole size appears to saturate at a shallow value independent of the burning laser power. To be more precise, defining $\Delta T = T_{ss} - T_i$, the relative change in transmission $\Delta T/T_i$ is 0.34. This seems large, but only because the sample is so strongly absorbing, $T_i = 0.023$. A better measure of hole depth is $\Delta\alpha/\alpha_i \equiv (\alpha_i - \alpha_{ss})/\alpha_i$. For Fig. 3, $\Delta\alpha/\alpha_i = 0.081$, indicating that roughly 8% of all centers stopped absorbing at the laser frequency. This fractional change in absorption constant varies from 0.05 to 0.3 for ReO_4^- in all the KI and RbI hosts studied.

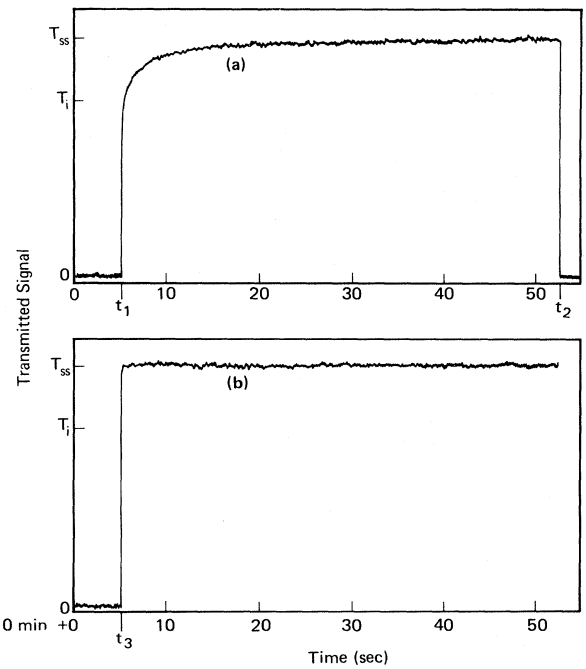

FIG. 3. Examples of persistent spectral hole growth. (a) After cooling a sample of RbI+0.8 mol% $KReO_4$ to 1.4 K in the dark, the CO_2-laser probe beam was unblocked at t_1. The initial sample transmission is given by T_i, and as the hole grows, the sample transmission approaches the steady-state value T_{ss}. The laser beam is again blocked at t_2. (b) After a dark period of 10 min, the probe beam is again unblocked at time t_3. $T_i = 0.023$, probe intensity, 150 μW/cm^2.

Curves like those presented in Fig. 3 also illustrate how persistent holes grow for the ReO_4^-—alkali-halide systems. The hole growth is nonexponential, showing a fast rate at small burning time and slower and slower rate as hole burning continues. Figure 4 shows the hole depth $\Delta\alpha/\alpha_i$ derived from data such as that in Fig. 3(a) versus burning time, with a *logarithmic* time axis. The data are not exactly described by log$t$, but a linear versus log plot removes more variation than any other standard plot. The growth of the hole is certainly slow, growing roughly like log$t$ at small times and appearing to saturate at large times. These novel growth curves will be discussed in Sec. IV.

An important question to ask is the following: How does the growth of the hole depend upon laser power? Given hole-growth curves such as Fig. 3, it is essentially impossible to unambiguously define a growth rate. Nevertheless, defining τ_g as the $(1/e)$-folding time for the approach of the sample transmission to steady state, then $(1/\tau_g)$ may be viewed as an effective growth rate. Figure 5 shows how $(1/\tau_g)$ depends on probe laser intensity. Even with these approximations, the effective growth rate appears to scale linearly with laser intensity, signifying that a one-photon process is responsible for the hole burning.

B. Hole erasing

By using one CO_2 laser to burn and monitor holes (the probe) and irradiating the sample with another CO_2 laser (called the pump), information may be obtained about

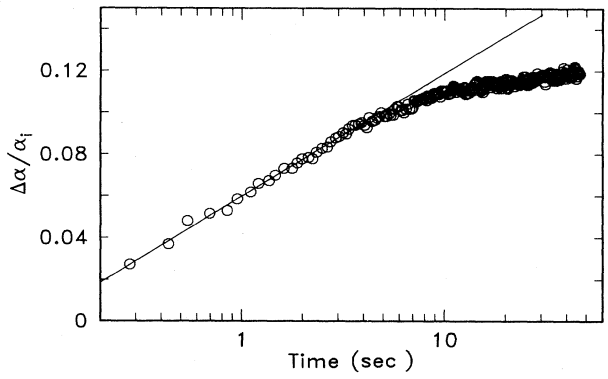

FIG. 4. Hole-growth data $\Delta\alpha/\alpha_i$ vs burning time for RbI+0.8 mol% $KReO_4$. The circles represent digitized values of the hole-growth data of Fig. 3. The solid line is a least-squares fit for small times. $L = 0.448$ cm, $\alpha_i = 7.519$ cm^{-1}, and the probe intensity is 150 μW/cm^2.

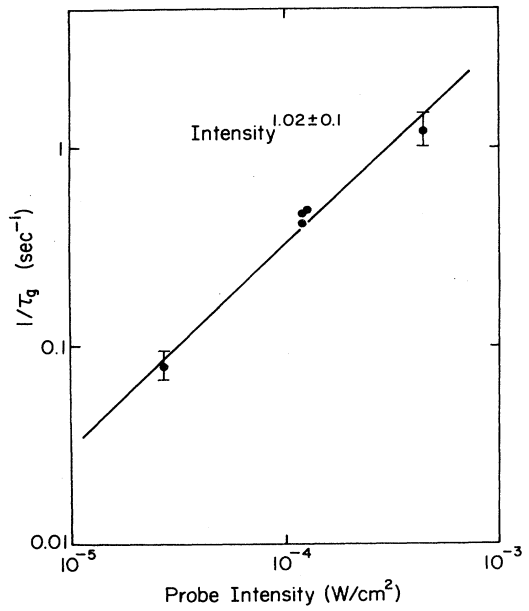

FIG. 5. Effective growth rate vs probe intensity for RbI:ReO_4^- at 1.4 K. The solid line is a least-squares fit to the data.

erasing of spectral holes in the ReO_4^-—alkali-halide system. Figure 6(a) shows the growth and simultaneous line-center detection of a hole burned by the probe laser, as described in Sec. II A and Fig. 3. If a second CO_2 laser (the pump) displaced by 10 MHz from the probe irradiates the sample for the time interval from t_2 to t_3, the hole burned by the probe is erased, as evidenced by the drop in

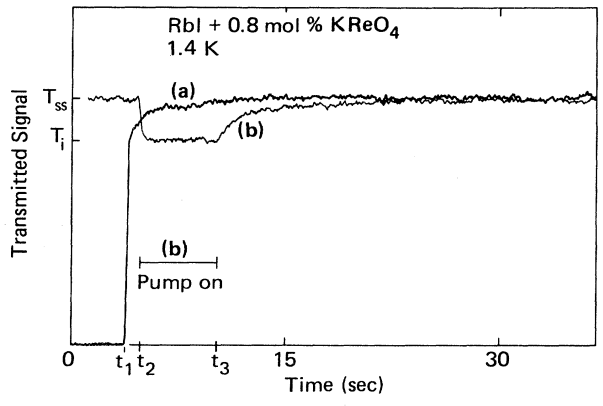

FIG. 6. Example of long-lived hole growth and erasing. (a) After cooling the sample from 77 to 1.4 K in the dark, the probe beam is unblocked at t_1. The probe transmission increases very slowly from T_i to T_{ss} over many seconds, indicating the growth of a hole burned by the probe. $T_i=0.02$. (b) After long exposure to the probe beam, the pump is unblocked at time t_2, erasing the probe hole, and blocked again at time t_3. The difference between the pump and probe frequencies is 10 MHz. The probe intensity is 100 μW/cm^2, and the pump intensity is 18 mW/cm^2.

probe transmission from T_{ss} to T_i [Fig. 6(b)]. When the pump laser is off, the probe transmission again rises to T_{ss}, signifying reburning of the probe hole. For the experimental situation in Fig. 6, the pump laser intensity is much higher than the probe intensity, so the probe hole is erased essentially completely. Of course, the pump is also burning a new hole centered at the pump frequency during this process.

This erasing phenomenon is a general feature of persistent holes in the ReO_4^-—alkali-halide system. In order to quantify this effect, measurements such as that depicted in Fig. 6 may be performed as a function of detuning Δf between the pump and probe frequencies. The fraction erased, F_e, is defined by $F_e \equiv \Delta T_e/\Delta T_{max}$, where ΔT_e is the steady-state probe transmission drop, and $\Delta T_{max} \equiv T_{ss} - T_i$, is the maximum erasable signal. (ΔT_{max} is also equal to the hole size at line center.) Figure 7 shows the dependence of F_e on detuning for two ratios of pump intensity to probe intensity. Identical curves result for negative values of Δf.

The shape of the F_e-vs-Δf curve is a result of the competing effects of the two lasers in producing hole burning. F_e is near zero for small Δf, grows to a maximum for $\Delta f = 10$—15 MHz, and then falls off for $\Delta f > 15$ MHz. To understand this, two regimes may be considered. First, for small Δf, the pump laser is burning a hole quite close to the probe frequency. (We recall that the probe has already burned a steady-state hole at $\Delta f = 0$ before the application of the pump.) When the powerful pump beam is applied, the probe team actually detects the transmission due to the hole *burned by the more powerful pump laser,* at a distance Δf from the pump frequency. In particular, at $\Delta f = 0$, the pump and probe holes overlap and $F_e = 0$. Thus the shape of Fig. 7 for Δf small should be expected to be a partial reflection of the (inverted) shape of the *pump* hole. Using this analysis, the (pump) hole appears to be on the order of 10 MHz wide.

For the case of Δf larger than the hole linewidth, the pump and probe holes do not overlap so strongly, and F_e

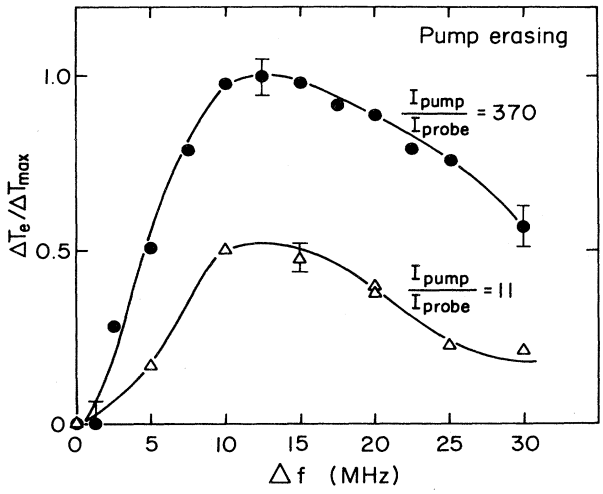

FIG. 7. Fraction erased, $F_e = \Delta T_e/\Delta T_{max}$ vs detuning Δf, between the pump and probe CO_2 lasers for ReO_4^- molecules in RbI. An identical curve results for negative values of Δf.

may be approximately viewed as the extent to which the probe hole is erased by the pump. At high ratios of pump power to probe power, the probe hole is essentially completely erased for $\Delta f \sim 10$—15 MHz. At lower pump powers, the fraction erased is correspondingly smaller. Of particular interest is the fact that an appreciable fraction of the probe hole can still be erased for Δf values as large as 30 MHz and larger. This shows that even for Δf so large that the pump and probe holes do not appreciably overlap, irradiation in the extreme wings of the probe hole can cause a redistribution of ground-state population and consequent partial erasure of the probe hole. A phenomenological model exhibiting this effect is presented in Sec. IV.

C. Hole line shape

Measurement of the persistent hole line shape presents some special problems, because exposure of the sample to a probe beam for any reasonable length of time causes a new hole to be burned at the probe frequency, thus altering the original line shape to be measured. The hole shape was measured in two completely different ways. Figures 8 and 9 show hole line shapes acquired using a diode laser probe and a CO_2-laser pump, and Fig. 10 shows line-shape measurements made with two CO_2 lasers.

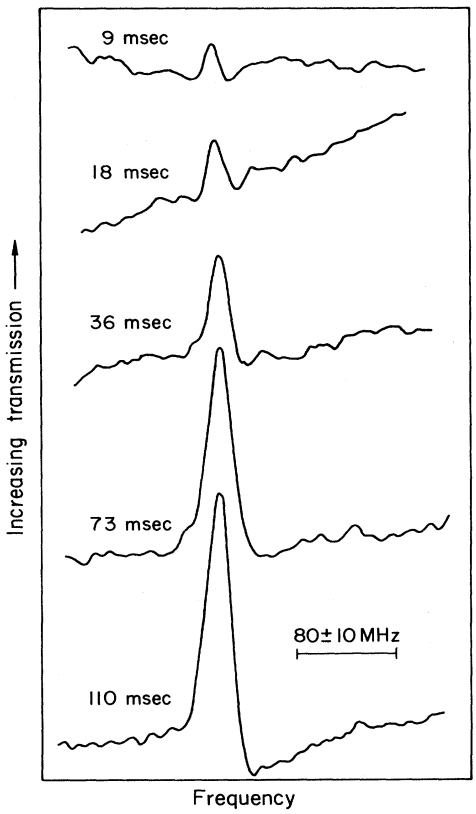

FIG. 8. Growth of the long-lived hole in KI:ReO_4^-:Rb^+ during the pump pulse. The pump pulse length is 120 msec. Each trace corresponds to a single diode laser spectrum of the sample transmission at the time delay shown from the beginning of the pump pulse. The five traces have been offset vertically for clarity.

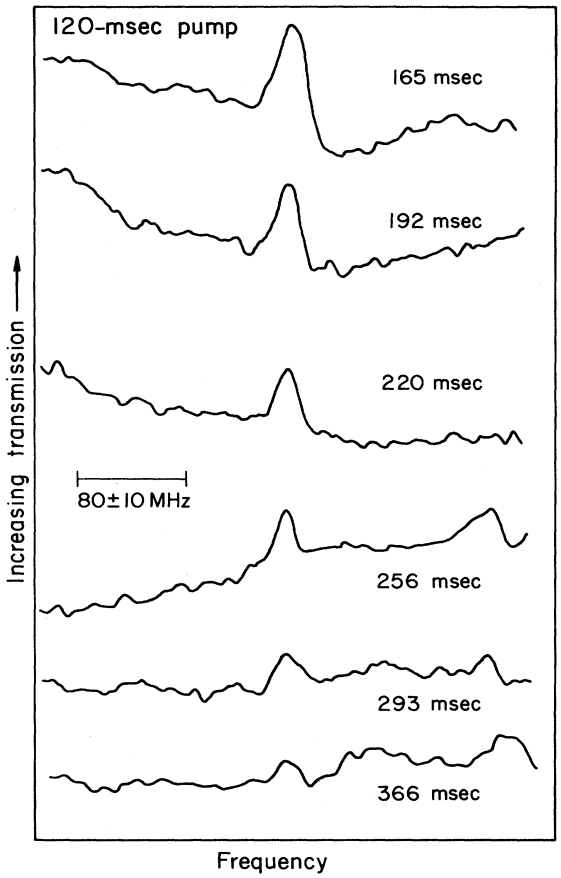

FIG. 9. Decay of the long-lived hole in KI:ReO_4^-:Rb^+ after termination of the 120-msec pump pulse. See Fig. 8. The time delay shown is measured from the beginning of the pump pulse.

Figures 8 and 9 present time-delayed hole spectra taken with a semiconductor diode laser as described in Sec. II B. Figure 8 shows the growth of a hole in the KI:ReO_4^-:Rb^+ system at 1.4 K. Each trace corresponds to a single scan of the frequency of the diode laser, with the y axis proportional to the sample transmission. The spectra have been acquired at various time delays from the beginning of the 120-msec-long pump pulse. The slanting baselines are artifacts due to low-frequency drifts and high-pass cutoff frequency (ac coupling). The partial dispersion shape in the trace for 110 msec is also an artifact, because the high-pass cutoff was set higher than optimal in order to achieve maximum signal to noise with minimum drift. These small inaccuracies do not obscure the main result that the persistent hole spectrum consists of a single, central hole, with width near 20 MHz. Since the frequency jitter of the diode laser itself was approximately 10 MHz, more accurate linewidths were measured with another technique (see Fig. 10). Nevertheless, one may safely conclude that the hole linewidth [full width at half maximum (FWHM)] is roughly equal to twice the true homogeneous width of the ReO_4^- transition in KI ($\Delta\nu_{hom}=9$ MHz, as measured by excited-state saturation[8]).

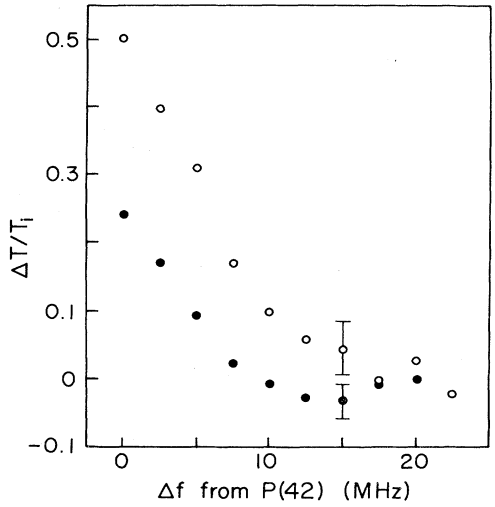

FIG. 10. Persistent hole line-shape measurements with two CO_2 lasers for RbI:ReO_4^-. The initial probe transmissions at $\Delta f=20$ and 22.5 MHz were averaged to define T_i. The pump intensity was 18 mW/cm^2, and the probe intensity was 100 μW/cm^2. The open and closed circles correspond to measurements at different sample locations.

Figure 9 shows hole spectra at various times after the end of the pump pulse. The hole certainly lasts much longer than the excited-state lifetime T_1 [~ 16 nsec (Ref. 8)]. The hole decays in ~ 250 msec, however, due to the continuous, sweeping irradiation by the probe laser. The hole decay produced by the scanning diode laser is roughly exponential in time,[6] with a rate that depends upon the power and the duration of the pump pulse that produced the hole.

Another method of measuring the persistent hole line shape is shown in Fig. 10. Here two CO_2 lasers are used to perform a point-by-point measurement of the increase in transmission corresponding to the formation of a hole in RbI:ReO_4^-. The pump laser is left on for a long time in order to burn a steady-state hole. Then the probe laser is unblocked at a fixed detuning, Δf, from the pump frequency. The *initial* probe beam transmission is recorded for each value of Δf, and these transmission measurements are plotted in Fig. 10 versus Δf. Since the hole is symmetric about the pump frequency, only positive values of Δf are plotted. The data show that the hole has a linewidth of 10 ± 2 MHz, which compares quite favorably with twice the homogeneous width of the transition.[8]

This section on hole line shapes may be summarized as follows. The hole spectrum consists of a single, central hole of width 10 ± 2 MHz in RbI and 20 ± 4 MHz in KI, which is essentially identical to the hole line shape for saturation holes.[8] The poor signal-to-noise ratio in the wings of the hole has not allowed the line shape to be conclusively characterized as Gaussian, Lorentzian, or some other shape. Furthermore, due again to signal-to-noise limitations and problems of accurate baseline determination, antiholes (or regions of increased absorption) were not observed in the wings of the hole.

D. Quantum efficiency

One important parameter of the hole-burning process is the quantum efficiency for persistent hole formation. The total infrared absorption at a fixed frequency is proportional to the number of centers within a homogeneous linewidth of that frequency. One possible definition of quantum efficiency is the number of centers that stop absorbing at the laser frequency divided by the total number of photons absorbed. The inverse of this efficiency would then be the number of photons required to cause one center to stop absorbing at the laser frequency. This is a time-independent definition only if the hole growth rate is constant, which is not the case for the ReO_4^- system (see Sec. III A). It would still be useful, however, to have a simple measure of quantum efficiency so that the probability of occurrence of this nonphotochemical process per photon per molecule can be compared with that for other photochemical and nonphotochemical systems. An approximate quantum efficiency, η_e, will now be defined and computed for the ReO_4^-—alkali-halide system.

The number of centers per unit volume within a homogeneous width of the laser frequency may be written $N(t)=N_0+\Delta N(t)$, where N_0 is the initial density before hole burning and $\Delta N(t)$ is the time-varying component. For instance, if the growth process were describable by a single exponential, $\Delta N(t)=-[1-\exp(-s_1 t)]$, where s_1 is the exponential growth rate. The effective quantum efficiency is given by the ratio of the initial rate of decrease of $N(t)$ to the rate of absorption of photons at $t=0$, or

$$\eta_e=\frac{-\left.\frac{dN(t)}{dt}\right|_{t=0} V}{\frac{P}{h\nu}(1-T_i-R)}, \tag{1}$$

where V is the volume of sample irradiated by the laser, P is the incident laser power, ν is the laser frequency, T_i is the initial sample transmission (external transmittance), R is the reflection loss, and h is Planck's constant. $dN(t)/dt$ is determined from a trace of sample transmission $T(t)$ such as in Fig. 3 as follows. With the use of Beer's law, $d\alpha/dt=-(TL)^{-1}dT/dt$, where α is the absorption coefficient and L is the sample length. dN/dt can be computed from $d\alpha/dt$ using the relation $\alpha=\sigma N$, where σ is the absorption cross section for molecules within a homogeneous linewidth of the laser frequency.

Calculation of η_e thus requires knowledge of the absorption cross section, σ. This parameter may be determined by using sum-rule techniques. The standard integrated absorption sum rule[9] can be written in the convenient form

$$S=\int \alpha(\tilde{\nu})d\tilde{\nu}=\frac{8\pi^3\tilde{\nu}_0}{ch}\frac{L}{n}\frac{|\vec{\mu}|^2}{3}N_{\rm tot}, \tag{2}$$

where n is the index of refraction, $L=[(n^2+2)/3]^2$, c is the speed of light, $\tilde{\nu}$ is the frequency in wave numbers (cm^{-1}), and $\tilde{\nu}_0$ is the frequency at the center of the band. $N_{\rm tot}$ is the density of absorbers producing the integrated absorption S. For ReO_4^- molecules in alkali halides, the

dipole moment determined from neutron activation measurements[6] is $|\vec{\mu}|^2 = 1.13(\pm 0.11)\times 10^{-37}$ (esu cm)^2. To determine σ, Eq. (2) can be applied to a Lorentzian homogeneous packet of width $\Delta\tilde{\nu} = (\pi c T_2)^{-1}$ at $\tilde{\nu}_0$ to obtain

$$\sigma = \frac{16\pi^3 T_2 \tilde{\nu}_0}{h}\frac{L}{n}\frac{|\vec{\mu}|^2}{3} = 2cT_2\left[\frac{S}{N_{\text{tot}}}\right], \tag{3}$$

where T_2 is the homogeneous transverse relaxation time.

These formulas may now be applied to the case of ReO_4^- molecules in alkali halides. With the use of the measured relaxation time (in RbI) $T_2 = 6.4\times 10^{-8}$ sec,[8] then $\sigma = 2.4\times 10^{-13}$ cm^2. From a typical hole growth measurement such as that in Fig. 3, $dT/dt = 0.12$/sec. At a pumping power of 220 nW in a spot with Gaussian radius 0.035 cm (sample length 0.11 cm), the efficiency η_e may be computed to be 2×10^{-3}. Values in the 10^{-3} range are typical of the ReO_4^- system, and are to be contrasted with the 10^{-5}–10^{-7} efficiencies that have been reported for nonphotochemical hole burning[1,2] in the visible. A high efficiency of 10^{-2} has been reported[3] for 1,2-difluoroethane in amorphous Ar. The quantum efficiency for ReO_4^- in alkali halides ranks among the largest measured efficiencies for persistent nonphotochemical hole burning in solids.

E. Temperature dependence

The lifetime of persistent holes in the ReO_4^-—alkali-halide system depends strongly upon temperature. If a sample containing a long-lived hole is warmed from 1.4 to 10—15 K in a few minutes and then cooled down to 1.4 K again, the long-lived hole disappears. If the sample is cycled to roughly 6 K and back down to 1.4 K, roughly 30% of the long-lived hole anneals away. At 4.2 K, the hole depth shows unmeasurable (less than 5%) decay during 2.5 sec of dark time. Quantitative measurements of hole lifetime as a function of temperature were not performed, due to the unavailability of the diode laser and other high-speed detection equipment at the time of the temperature-dependent studies. It is not unreasonable to assume, however, that the hole lifetime is on the order of minutes at ~ 6 K, and considerably less than 1 min at ~ 10 K. Future studies of this system should include a thorough investigation of lifetime as a function of temperature.

This reduced hole lifetime complicated the temperature-dependent measurements of hole linewidth and hole depth. Figure 11 shows the temperature dependence of the persistent hole linewidth for the $KI:ReO_4^-:Rb^+$ system. These data were derived from diode laser scans of the hole line shape each taken within 2 msec after the termination of a pump CO_2-laser pulse of intensity less than $0.1I_s$. The linewidth is roughly constant up to ~ 8 K, and then the linewidth grows very rapidly. This temperature dependence mirrors that for saturation holes presented in Ref. 8. The increasing linewidth at temperatures greater than 10 K may be attributed to phonon scattering processes.

The pump erasing phenomenon described in Sec. III B allows a steady-state measurement of the hole depth,

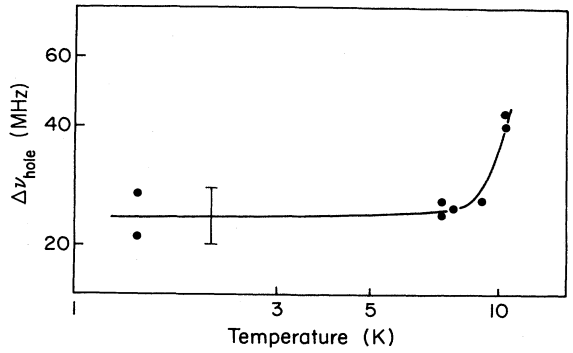

FIG. 11. Temperature dependence of the linewidth (FWHM) of persistent holes in $KI:ReO_4^-:Rb^+$. The solid line is a guide to the eye.

$\Delta T/T_i$, at any temperature. The reasonable (and experimentally verified) assumption is made that the high-power CO_2 pump at $\Delta f = 10$ MHz completely erases the probe CO_2 hole, allowing the value of T_i for the probe beam to be easily measured. The growth of the probe transmission from T_i to T_{ss} then allows the hole depth at a given temperature Θ to be easily measured. Contrary to expectations, the hole depth does not exhibit an Arrhenius behavior. Figure 12 shows that the data follow the function $\exp(-\Theta^2/\Theta_c^2)$, with $\Theta_c \approx 5$ K. Since the hole

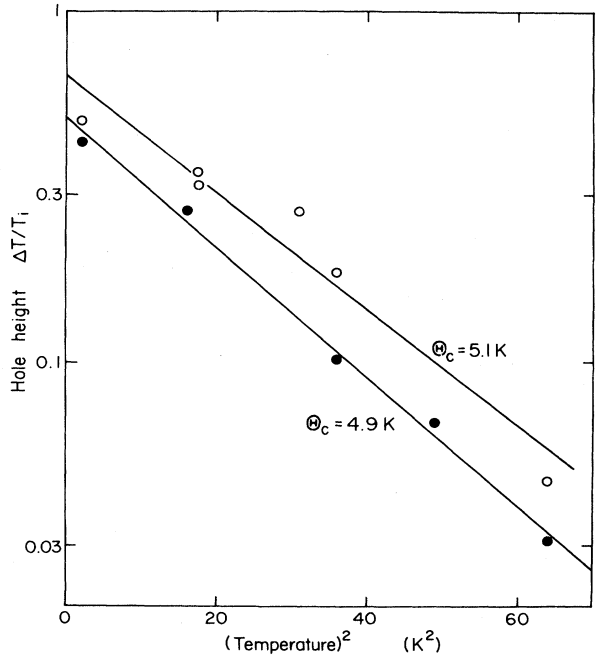

FIG. 12. Temperature dependence of the long-lived hole depth for $RbI:ReO_4^-$. The hole depth $\Delta T/T_i$, derived from pump erasing experiments at $\Delta f = 10$ MHz, is plotted vs the temperature squared. The open and closed circles refer to two different runs. The solid lines are least-squares fits to the data as described in the text.

linewidth is constant up to ~ 10 K, the area under the persistent hole also falls with temperature according to $\exp(-\Theta^2/\Theta_c^2)$.

F. Concentration dependence

Of particular interest in the determination of the underlying physics of the long-lived hole is the concentration dependence of the hole depth. Unfortunately, the doped RbI crystals have strong gradients of ReO_4^- concentration, so that a measurement of the hole height and a subsequent neutron activation measurement of the ReO_4^- concentration in the same sample region is virtually impossible. However, what can be easily measured is the initial absorption before a hole can grow, α_i, and the hole depth $\Delta\alpha$. With the use of the fact that the inhomogeneous width is independent of doping level and making the reasonable assumption that the cross section σ for the ν_3 mode absorption is also independent of doping level, α_i is directly proportional to the local ReO_4^- concentration.

Figure 13 displays values of $\Delta\alpha$ and α_i for several different samples. The various values of α_i shown for the same sample were derived from measurements at different positions. The straight line is a least-squares fit to the data with slope 0.8 ± 0.2. The approximately linear dependence of $\Delta\alpha$ on α_i suggests that the long-lived hole depth is linear in ReO_4^- concentration over a 30-fold range. This implies that the mechanism for formation of the long-lived hole is intrinsic to single ReO_4^- molecules.

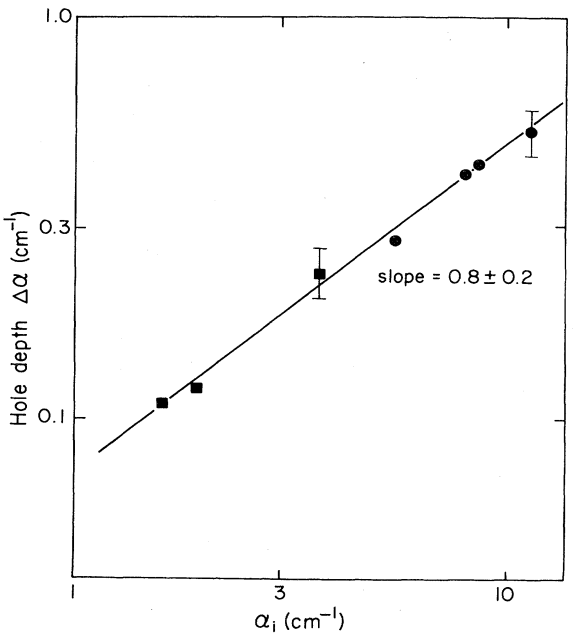

FIG. 13. Concentration dependence of the long-lived hole depth. The circles correspond to measurements on an annealed sample of RbI+0.8 mol% $KReO_4$. The squares represent measurements on unannealed RbI+0.4 mol% $KReO_4$. In all cases, T_i and T_{ss} were measured by using a pump CO_2 laser at $\Delta f = 10$ MHz to erase the probe hole. The straight line is a least-squares fit to the data.

Concentration-dependent processes such as vibrational energy transfer are not important for this system.

G. Frequency dependence within the inhomogeneously broadened line

Since the inhomogeneously broadened ν_3 mode absorption is 1—2 cm^{-1} in width in the RbI and KI:Rb^+ hosts, a natural question to ask is whether or not holes can be burned at frequencies other than the 10.8 μm $P(42)$ CO_2-laser line. Hole-burning experiments with a single diode laser were performed to answer this question. The laser frequency was held fixed for 1 sec to burn a hole, then repetitively scanned across the hole at a 1-kHz rate. Because the scanning diode laser also erases the hole, the first laser scan after the burn period was stored in a digital oscilloscope. This entire process was repeated 32 times and the resulting scans were averaged.

In order to try to burn holes at line center, lightly doped samples were grown. For RbI+0.001 mol% $RbReO_4$, line center for the ^{185}Re isotope is ~ 0.2 cm^{-1} below the CO_2 line $P(44)$ at 1.4 K. Attempts to burn holes with the diode laser on the sides or at the center of this line were unsuccessful. In addition, hole burning was attempted at the $^{187}ReO_4^-$ line center for a sample of KI+0.001 mol% $KReO_4$, 0.2 cm^{-1} above $P(42)$. Once again, no long-lived holes were observed. Finally, hole burning was attempted over a 0.1-cm^{-1} range near $P(42)$ in a sample of RbI+0.8 mol% $KReO_4$. The hole depth was observed to decrease for burning frequencies closer to line center.

These results show that the long-lived hole-burning phenomenon is somehow associated with the absorption in the wings of a strongly inhomogeneously broadened line. In the case of RbI+0.8 mol% $KReO_4$, long-lived hole burning is strongest in a 0.1-cm^{-1} region near $P(42)$, ~ 2.2 cm^{-1} from line center, and for KI+0.005 mol% $KReO_4$+2.5 mol% RbI, hole burning is strongest near $P(42)$, 0.2 cm^{-1} from line center. This property of persistent holes in the ReO_4^-—alkali-halide systems suggests that the hole-burning mechanism is associated with the larger values of strain found in the wings of the inhomogeneously broadened line.

H. Stark effects

For a tetrahedral molecule at a perfectly cubic lattice site, no first-order Stark effect can occur. However, hole-burning spectroscopy allows studies of very weak Stark effects to be done inside the inhomogeneous line at extremely high resolution. Unfortunately, diode lasers were not available for these experiments. Consequently, the technique that was used involved monitoring the total transmission of a single CO_2-laser probe beam during the application of electric fields to the sample. The electric field was applied along the [010] axis of a sample of RbI+0.8 mol% $KReO_4$. The infrared beam propagated along [001], and was polarized either parallel ($\vec{E}_{ir}||[010]$) or perpendicular ($\vec{E}_{ir}||[100]$) to the dc field $\vec{E}_{dc}$.

In a typical experiment, a persistent hole was burned in the sample using the probe laser, causing the sample transmission to reach T_{ss}. Then various electric fields

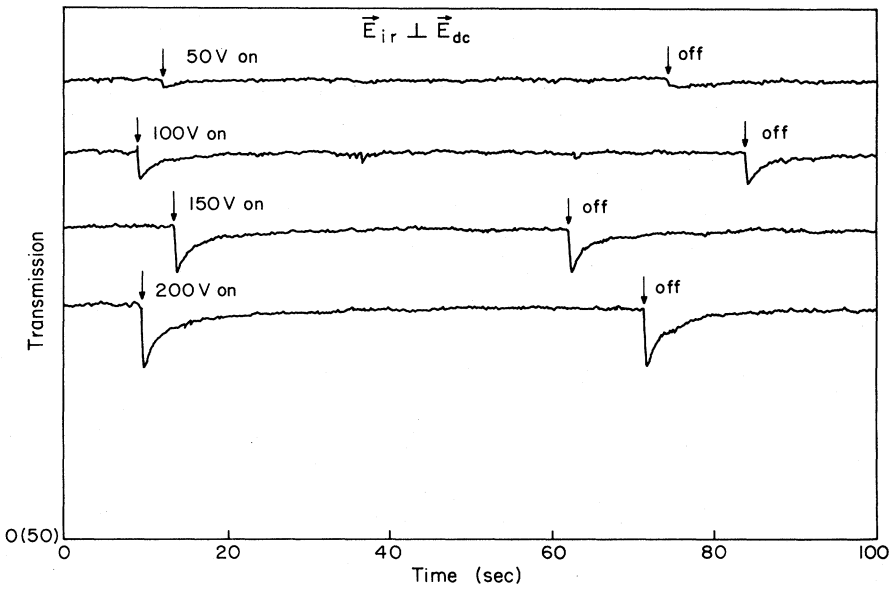

FIG. 14. Example of results from electric field experiments. Each of the four traces corresponds to the time-dependent sample transmission of annealed RbI+0.8 mol% $KReO_4$ at 1.4 K. The zero line in the figure is appropriate for the uppermost trace, and the other three traces have been shifted downward for clarity. The arrows mark the instants of application and removal (grounding) of the electric field across the sample. For a plate gap of 0.35±0.05 cm, the corresponding electric fields are 50 V—140 V/cm, 100 V—290 V/cm, 150 V—430 V/cm, and 200 V—570 V/cm.

were applied in a step-function fashion and the change in sample transmission was recorded. For $\vec{E}_{ir}||\vec{E}_{dc}$, no effect was observed for electric fields up to 600 V/cm. Figure 14 shows the interesting effects observed for the orthogonal case, $\vec{E}_{ir}\perp\vec{E}_{dc}$. For small fields, a small drop in transmission occurs upon application of the field, followed by a slow recovery of the transmission to T_{ss}. Removal of the field produces a similar transient. As the applied field is increased, the transmission drop grows, and the transient at field removal is very similar to the transient at initial field application.

These results suggest that the electric field shifts or splits the absorbing frequency of the centers interacting with the probe beam. After application of the field, the laser is interacting with a new set of centers, within which a long-lived hole has not yet been established. The probe laser then burns a hole in the absorption of these new centers, producing the slow growth of the transmission observed after the initial drop. The growth of this new hole appears to erase the original hole, because when the original centers are brought back into resonance with the laser, the original hole regrows.

Several experiments were performed to more fully characterize this process. The basic properties of the effect are as follows.

(a) For $\vec{E}_{ir}||\vec{E}_{dc}$, analyzer axis $||\vec{E}_{ir}$, no observable transmission drop occurs as stated above.

(b) For $\vec{E}_{ir}\perp\vec{E}_{dc}$, analyzer axis $||\vec{E}_{ir}$, large transmission drops occur as shown in Fig. 14. Furthermore, no hysteresis occurs. Application of fields up to 570 V/cm in 130 V/cm increments produces small drops in transmission at each step, going up or down, for positive or negative voltages. The transmission drop saturates above 570 V/cm.

(c) For $\vec{E}_{ir}\perp\vec{E}_{dc}$, analyzer axis $\perp\vec{E}_{ir}$, no signal is observed above the rejection level of the polarizer. In other words, application of electric fields does not depolarize the probe beam.

Figure 15 shows the complete field dependence of the relative transmission drop, $\Delta T/T_{ss}$. The lack of effect at low fields can be interpreted as a frequency shift or splitting of the ν_3 mode that is too small to affect the height of the original hole appreciably. For fields ≥ 600 V/cm, the laser is forced to interact with totally fresh centers with initial total transmission near T_i.

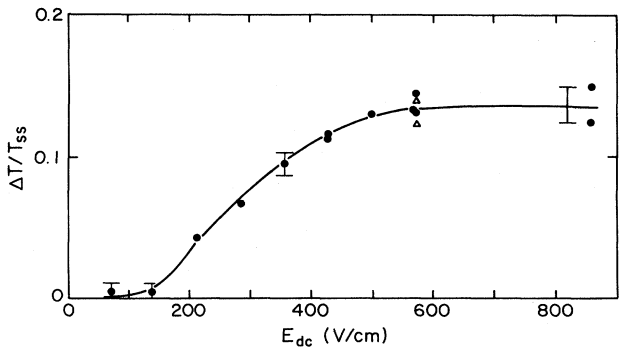

FIG. 15. Relative transmission change $\Delta T/T_{ss}$ vs electric field. For this sample of RbI+0.8 mol% $KReO_4$, $T_{ss}=0.12$, and the laser intensity is 100 $\mu W/cm^2$. The peak height of the long-lived hole is $\Delta T/T_{ss}=0.15$.

These results can be interpreted in the following manner. The infrared beam interacts with transitions with induced ν_3 dipole moments parallel to the infrared electric field. These centers appear to have a small permanent dipole that is *perpendicular* to the infrared electric field. The size of this dipole can be estimated from the known line shape of the long-lived hole and the data in Figs. 15 and 10. 300 V/cm is sufficient to shift the hole an estimated 5 MHz, so the permanent dipole has an estimated value of 3.3×10^{-20} esu cm. This dipole can be associated with a small local departure from perfect symmetry, but why the ground-state population of the transition polarized perpendicular to this dipole depends upon the Stark energy of the dipole is unknown at present.

I. Other properties

The persistent hole height and line shape do not depend upon the relative polarizations of the burning and probing beams.[6] In other words, if a hole is burned in one polarization, a hole is also formed in the perpendicular polarization. This result is consistent with the triply degenerate ν_3 mode excited-state symmetry. A given redistribution of the ground-state population carries no memory of the polarization of the ν_3 mode excited state that was used to achieve redistribution.

Application of rf magnetic fields up to 0.1 G in the frequency range 2.5—60 MHz has no observable effect on the long-lived hole.[6] This suggests that the formation of persistent holes is not due to optical pumping of nuclear quadrupole levels[10] of the spin-$\frac{5}{2}$ ^{185}Re and ^{187}Re nuclei (quadrupole moments 2.7 and 2.6 b, respectively). Either there are no electric field gradients to split the nuclear quadrupole levels of the ground state, or there is a broad, continuous distribution of field gradients at the ReO_4^- sites.

No paraelectric resonance absorption is observed in the range 26—40 GHz for ReO_4^- molecules in the RbI or KI:Na^+ hosts.[6,11] This casts doubt on the possibility of local distortions of the ReO_4^- environment sufficient to produce electric dipole moments greater than 0.1 D. This result makes the existence of a static Jahn-Teller distortion and associated electric field gradients relatively improbable.

J. Summary

This section summarizes the properties of persistent holes in the ν_3 mode absorption of ReO_4^- molecules in alkali-halide hosts. All properties were measured at 1.4 K unless otherwise stated.

(a) Persistent holes have been burned in the inhomogeneously broadened ν_3 mode absorption of ReO_4^- molecules in a variety of doubly and singly doped KI and RbI crystals. The observation of long-lived holes does not appear to depend upon sample annealing.

(b) Holes have only been observed at or near $P(42)$, $\sim$2.2 cm from the $^{185}ReO_4^-$ line center in RbI, and 0.22 cm^{-1} from the $^{187}ReO_4^-$ line center in the KI hosts. Long-lived holes cannot be burned with the diode laser in the immediate region of the ν_3 mode line center in either KI+0.001 mol % $KReO_4$ or RbI+0.001 mol % $RbReO_4$.

(c) The long-lived hole spectrum consists of a single, central hole only. The poor signal-to-noise ratio in the wings of the hole has not allowed the line shape to be conclusively identified as either Gaussian or Lorentzian. No antiholes larger than 5—10 % of the hole height have been observed in the wings of the hole.

(d) The linewidth of the long-lived hole is approximately the same as the linewidth of the transient saturation hole.

(e) The long-lived hole is persistent at 1.4 K in conventionally annealed samples, showing no decrease in amplitude after 10 min in the dark. The lifetime may be much longer.

(f) The long-lived hole depth saturates after long exposure to the burning beam. Steady-state values of $\Delta\alpha/\alpha_i$ range from 0.05 to 0.3.

(g) The time dependence of long-lived hole growth is not exponential, nor is it described by a power law. The growth appears to be characterized by a continuously changing rate which is fast at small times and slow at large times. The growth is roughly logarithmic at small times, and less than logarithmic as steady state is reached. The effective growth rate $1/\tau_g$ depends linearly upon the burning beam intensity.

(h) The hole height and line shape do not depend upon the relative polarizations of the burning and probing beams.

(i) A hole burned by one laser can be erased to varying degrees by a second laser at detuning Δf. After erasing, the regrowth rate of the long-lived hole $1/\tau_g$ depends on Δf. For detunings in the (10—15)-MHz range, probe intensity 100 $\mu W/cm^2$, and erasing beam intensities ≥ 20 mW/cm^2, the erasing process is 100% efficient, i.e., the sample transmission is reduced to the pristine, no-hole value, T_i.

(j) The long-lived hole depth $\Delta\alpha$ is linear in the total absorption in the absence of the hole, α_i. This suggests that the hole depth is linear in the concentration of ReO_4^- molecules in the sample, and that single, isolated ReO_4^- molecules are responsible for the hole-burning process.

(k) Temperature dependence:

(i) The long-lived hole spontaneously anneals at sample temperatures above $\sim$10 K.

(ii) The long-lived hole height depends upon temperature Θ, as $\exp-(\Theta^2/\Theta_c^2)$, with $\Theta_c\sim5$ K.

(iii) The hole width is independent of temperature for $\Theta<10$ K, and grows very quickly for $\Theta>10$ K.

(l) Erasing by a scanning diode laser: The hole decay produced by a scanning diode laser is exponential in time, with a rate that depends upon the power and the duration of the pump pulse that produced the hole.[6]

(m) dc electric fields applied parallel to the polarization vector of the burning beam have no observable effect on the hole. Fields applied perpendicular to the infrared field instantly erase part of the long-lived hole, and then a new hole grows under the influence of the infrared beam. The erasing depth is zero for small dc fields, and saturates at complete erasing for fields >600 V/cm. This process shows no hysteresis and is reversible if the dc field is applied and removed in the dark.

(n) Application of rf magnetic fields in the range 2.5—60 MHz has no observable effect on the long-lived hole.

(o) Paraelectric resonance experiments in the range 26—40 GHz show no measurable absorption.

Any future models of long-lived hole burning for the ν_3 vibrational mode of ReO_4^- molecules in alkali halides must provide the mechanisms responsible for these various properties.

IV. DISCUSSION

A. Microscopic model

A natural configuration for the ReO_4^- molecule substituted for the halide ion in an alkali-halide crystal is with the four tetrahedral Re—O bonds directed along four of the eight available ⟨111⟩ directions. Indeed, careful studies of the infrared and Raman spectra of ReO_4^- molecules in alkali halides[12] indicate that the symmetry of the ReO_4^- molecule in the solid is still tetrahedral to high accuracy. Furthermore, steric effects are expected to be important, because the ionic radius of the molecule [2.7 Å (Ref. 6)] is larger than the ionic radius of the halogen for which the molecule substitutes (I^-—2.19 Å). Examination of an ionic model for the lattice with the ReO_4^- at the halide ion site shows that the steric pressure from nearby ions is somewhat relieved if the Re—O bonds lie along ⟨111⟩ body diagonals.

The molecular ion thus may be expected to have two configurations in the lattice related by a $\pi/2$ rotation about a ⟨100⟩ axis. These two configurations are conceptually equivalent to the two ways in which a tetrahedron (with symmetry group T_d) can be inscribed in a cube (with symmetry group O_h). Steric effects can be expected to produce a high barrier to rotation between the two configurations and infrared spectroscopy of the ν_3 mode absorption (over a 0.2-cm^{-1} range[7]) suggests that there are no strong librational absorptions at low temperatures, in contrast to the situation for CN^- molecules in alkali halides,[13] for instance.

Figure 16 shows the expected energy-level diagram. The two ground-state configurations are denoted A and B, and they are connected by a configurational coordinate, θ. The two configurations may be expected to differ in energy by an amount ϵ, which is proportional to an appropriate component of the elastic strain gradient due to nearby defects. The upper wells correspond to the excitation of one quantum of the ν_3 vibrational mode. Owing to the symmetry of the ν_3 vibration (T_2) and consistent with the absence of strong phonon sum bands at low temperatures, there is no Franck-Condon shift. However, due to the weak interaction of the ν_3 mode and the strain field, the strain-induced inequivalence (ϵ^*) for the excited state is assumed different from that in the ground state by an amount $\hbar\Delta \equiv \epsilon^* - \epsilon$. This strain inequivalence is the mechanism whereby the infrared absorption frequency for molecules in configuration A differs from that for molecules in configuration B. The observation of strong persistent holes only in the wings of the inhomogeneously broadened line supports this assumption. The energy levels in the inequivalent wells represent possible excitation of librational modes of the ReO_4^- molecules about the equilibrium configuration. In order to achieve a long lifetime in a given well at 1.4 K, tunneling or phonon-induced reorientation are assumed to be too weak to allow reorientation in the librational ground state.

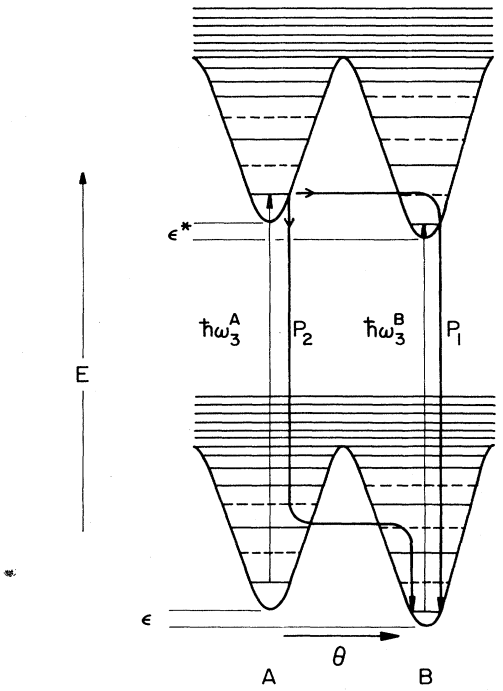

FIG. 16. Potential energy diagrams for the ReO_4^- spherical-top molecule in the ground and excited ν_3 mode vibrational states. Two possible configurations A and B occur for each state.

Various mechanisms for photoinduced reorientation may now be described. Pathway P_1 in Fig. 16 consists of the following steps: photoexcitation in well A, configurational tunneling to the new configuration B while in the optically excited state, and subsequent relaxation to the ground state of the alternate configuration. This mechanism is very similar to that proposed by Hayes, Stout, and Small to explain nonphotochemical hole burning for electronic transitions of molecules in glasses.[1] The principal difference is that for the ReO_4^- system, the configurational degeneracy is provided by the optically active site itself rather than by the presence of nearby tunneling systems in the host matrix. For neither the ReO_4^- system nor the glass system of Hayes, Stout, and Small is there an evident reason why reorientation or tunneling should be easier in the optically excited state compared to the ground state. The hole burning described here is entirely within a zero-phonon line, so the various librationally excited levels in the ν_3 mode excited state are not accessible.

A more probable mechanism for hole burning is pathway P_2: excitation in configuration A, nonradiative relaxation to an excited librational level in the vibrational ground state of well A, subsequent tunneling in this librational state to well B, and finally relaxation to the new

ground state. This pathway is more natural because it does not require more efficient tunneling from one configuration to another in the vibrational excited state compared to the ground state. This process should be important for the glass systems as well.

In any case, the consequence of molecular reorientation is to shift the infrared absorption at any particular active site from $\hbar\omega_3^A$ to $\hbar\omega_3^B$ where $\hbar\omega_3^B-\hbar\omega_3^A=\hbar\Delta=\epsilon^*-\epsilon$. Conversely, if the initial configuration of the molecule were orientation B and $\hbar\omega_3^B$ were in resonance with the laser energy, the optical absorption would shift from $\hbar\omega_3^B$ to $\hbar\omega_3^A$ by an amount $-\hbar\Delta$. The probability for either process would be determined by the microscopic branching ratios of pathways P_1 and P_2 relative to the return to the initial ground state without reorientation. Calculation of these branching ratios is outside the scope of this paper, because of the complexity of the vibrational decay process.[8]

B. Phenomenology

With the use of the ideas presented in Sec. IV A, a simple rate equation model for the photon-induced reorientation process may be formed. (A somewhat related kinetic photo-orientation model for electronic transitions of PO_2^- molecules in KCl has appeared elsewhere.[14]) This phenomenological model can be used to calculate the expected hole line shape and hole-growth curves, which may then be compared with the experimental data.

The basic assumption of the model is that the probability of reorientation for a given center is proportional to the absorption produced by the center at the frequency of the burning laser, ω_p. Each center is characterized by two parameters: the difference in optical absorption energies for the two configurations $\hbar\Delta$ and the mean frequency $\bar{\omega}=(\omega_3^A+\omega_3^B)/2$. For the A configuration, the absorption from the center at a frequency ω given by a normalized line shape $f(\omega-\omega_3^A)$, and for the B configuration by a line shape centered at ω_3^B, $f(\omega-\omega_3^B)$. The fundamental quantity of the model is the probability that the center is in the the A orientation, $\beta(\bar{\omega})$. Before any pumping light irradiates the sample, the orientation probability $\beta(\bar{\omega})=\frac{1}{2}$ for all values of $\bar{\omega}$ (all centers). The effect of the pumping light is to change the distribution of the centers among the two orientations A and B. The basic rate equation then becomes

$$\frac{d\beta(\bar{\omega})}{dt}=P[1-\beta(\bar{\omega})]f(\omega_p-\bar{\omega}-\Delta/2) \\ -P\beta(\bar{\omega})f(\omega_p-\bar{\omega}+\Delta/2)\ , \tag{4}$$

where P is a measure of the pumping rate. It is proportional to the pumping power, to the absorption cross section, and to the burning efficiency η mentioned earlier. This is simply a statement that if the center is in orientation A and absorbs a photon from the laser at ω_p, then a reorientation occurs (with probability η) and vice versa if the center is in orientation B. Thus if ω_3^A and ω_3^B are not symmetrically displaced about ω_p, the pump produces a net reorientation into the state farther from the pump frequency ω_p.

Equation (4) may be solved in the steady state to yield expressions for the hole line shape and in the transient regime to predict the hole growth. The condition for steady state is $d\beta(\bar{\omega})/dt=0$, or equivalently that centers be excited by the pump from each of the configurations at the *same* rate:

$$\beta(\bar{\omega})f(\omega_p-\bar{\omega}+\Delta/2)=[1-\beta(\bar{\omega})]f(\omega_p-\bar{\omega}-\Delta/2)\ . \tag{5}$$

For a given functional form for $f(\omega)$, Eq. (5) may be easily solved for $\beta(\bar{\omega})$. The total absorption at frequency ω, if $\alpha_0(\omega)$ defines the distribution of mean frequencies $\bar{\omega}$ of the A,B pairs, is produced simply by summing the absorption contributions from all possible values of Δ and $\bar{\omega}$ (in the presence of the pumping light)

$$\alpha_p(\omega)=\int_{-\infty}^{\infty}\alpha_0(\bar{\omega})d\bar{\omega} \times\int_{-\infty}^{\infty}g(\Delta)d\Delta \times\{\beta(\bar{\omega})f(\omega-\bar{\omega}+\Delta/2) +[1-\beta(\bar{\omega})]f(\omega-\bar{\omega}-\Delta/2)\}\ , \tag{6}$$

where $g(\Delta)$ is a normalized distribution function for Δ.

Physical insight allows certain simplifications of this integral. Since the persistent hole widths are the same as that for the transient saturation holes, the Δ distribution cannot be broader than the width of the line-shape function f. This fact was verified directly by assuming both a constant splitting of Δ_1 for all centers and a Lorentzian splitting distribution and numerically evaluating the complete double integral. In both cases, assuming a Δ distribution (or a value of Δ_1) that is larger in width than $f(\omega)$ produces holes that are larger than the transient saturation holes. Thus the Δ distribution may be safely assumed to be narrower than the line-shape function, f. If $\beta(\bar{\omega})$ is obtained from Eq. (5) and substituted in Eq. (6), and if $\alpha_0(\omega)$ is assumed broad compared with $f(\omega)$ (strong inhomogeneous broadening), the hole line shape becomes

$$\frac{\alpha_0(\omega)-\alpha_p(\omega)}{\alpha_0(\omega)}=\frac{\langle\Delta^2\rangle}{4}\int_{-\infty}^{\infty}\frac{d\bar{\omega}}{f(\omega_p-\bar{\omega})}\frac{df(\omega_p-\omega)}{d\bar{\omega}} \times\frac{df(\omega-\bar{\omega})}{d\bar{\omega}}\ . \tag{7}$$

Here, $\langle\Delta^2\rangle=\int_{-\infty}^{\infty}g(\Delta)\Delta^2d\Delta$ is the mean-square size of the inequivalence splitting. For the time dependence, Eq. (4) may be easily integrated to give $\beta(\bar{\omega},t)$ which can then be used in Eq. (6) to compute the growth of the hole at its center, $\omega=\omega_p$.

To generate hole line shapes and growth curves that may be compared with measured data, a Lorentzian form for f is assumed: $f(\omega)=(\Gamma/\pi)(\omega^2+\Gamma^2)^{-1}$ where Γ is the homogeneous radian halfwidth. Then the steady-state value of $\beta(\bar{\omega})$ is given by

$$\beta_{ss}(\bar{\omega})=\frac{\bar{\omega}\Delta}{\Gamma^2+\bar{\omega}^2+\Delta^2/4}\ . \tag{8}$$

The hole line shape follows from a trivial contour integration of Eq. (7)

$$\frac{\alpha_0(\omega)-\alpha_p(\omega)}{\alpha_0(\omega)}=\frac{\langle\Delta^2\rangle}{2}\frac{d}{d\omega}\left[\frac{\omega}{\omega^2+4\Gamma^2}\right]. \tag{9}$$

Figure 17 shows the result for $\Gamma=1, \langle\Delta^2\rangle=0.1$. The following observations may be made.

(1) The steady-state hole depth at the center of the hole is equal to $\langle\Delta^2\rangle/8\Gamma^2$. Thus the hole is shallow for $\langle\Delta^2\rangle<\Gamma^2$, and the depth is independent of pump power level. In particular, the finite hole depth is *not* a consequence of "two kinds of centers—burnable and nonburnable," but rather it is a natural consequence of the model with $\langle\Delta^2\rangle$ small. Furthermore, the holes are expected to be deeper in the wings of the inhomogeneous line, because $\langle\Delta^2\rangle$ is larger there.

(2) For $\langle\Delta^2\rangle<\Gamma^2$, the steady-state hole width is essentially equal to the homogeneous width of the transition, independent of the magnitude of the pumping power.

(3) The hole line shape is not Lorentzian, but has associated with it shallow, broad wings of *increased* absorption, or antiholes.

(4) Erasure of the hole by irradiation at a frequency in the wings of the hole follows directly from the model. In addition, the model predicts decreased efficiency for this erasure as the displacement of the erasing frequency from the center of the hole is increased.

(5) At low temperatures, the steady state is a competition between rwo radiation-stimulated processes, not between a radiation-stimulated process and thermal erasing. Hence the holes would be expected to persist in the dark.

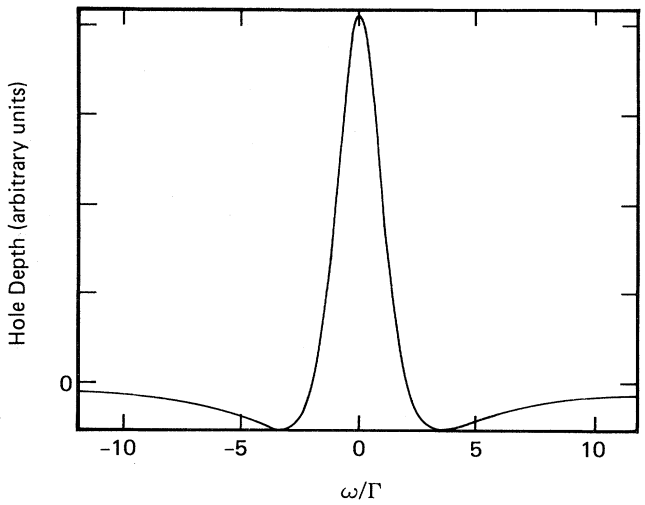

FIG. 17. Hole line shape for the typical case $\Delta \ll \Gamma$. Positive hole depth corresponds to *decreased* absorption (hole). $\Gamma=1, \langle\Delta^2\rangle=0.1$.

The experimental results of Sec. III easily verify points 1, 2, 4, and 5. Considering point 3, the direct line-shape measurements of Sec. III C possess insufficient signal-to-noise ratio to verify the existence of broad antiholes in the wings of the holes. Nevertheless, we conclude that this phenomenological model describes the steady-state properties of the persistent hole reasonably well.

Turning now to the time dependence of the hole, the rate equation, Eq. (4), may be integrated for a Lorentzian homogeneous line shape f to yield (with $\omega_p=0$)

$$\beta(\bar{\omega},t)=\beta_{ss}(\bar{\omega})\left\{1-\exp\left[\frac{-tP\Gamma}{\pi}\left[\frac{1}{(\bar{\omega}+\Delta/2)^2+\Gamma^2}+\frac{1}{(\bar{\omega}-\Delta/2)^2+\Gamma^2}\right]\right]\right\}. \tag{10}$$

This expression may be substituted into Eq. (6) to compute the growth of the hole. For optically thick samples, the pumping parameter P is larger at the front of the sample than at the back. We thus take Eq. (10) to apply to a thin slice dx of the sample at a position x from the input face and write $P(x)=P_0\exp(-\alpha_i x)$, where P_0 is a constant. This is not a self-consistent solution to the problem, because the sample absorption α_i is also taken to be as a constant. Nevertheless, for shallow holes, the assumption of constant absorption in the calculation of $P(x)$ is quite reasonable.

The complete hole growth may now be calculated by using Eq. (6) and integrating over all slices of sample from 0 to the sample length L. Again making the reasonable assumption that the Δ distribution is narrower than $f(\omega)$, and further choosing to calculate the hole growth at $\omega=\omega_p=0$ yields

$$\frac{\alpha_0(0)-\alpha_p(0,t)}{\alpha_0(0)}=\frac{\langle\Delta^2\rangle}{8\Gamma^2}\left\{1-\frac{8\Gamma^3}{\pi L}\int_0^L dx\int_{-\infty}^{\infty}d\bar{\omega}\frac{\bar{\omega}^2}{(\bar{\omega}^2+\Gamma^2)^3}\exp\left[\frac{-2tP(x)\Gamma}{\pi}\left[\frac{1}{\bar{\omega}^2+\Gamma^2}\right]\right]\right\}. \tag{11}$$

The essential physics of the model is evident from an inspection of this integral. The hole growth is clearly not described by a single exponential. In fact, the total hole growth is described by a sum over many exponentials corresponding to classes of centers further and further from resonance with the burning light. The centers close to the laser frequency ($\omega_p=0$) will reach steady state quickly, while those centers at larger detunings have larger time constants. Thus, at small times, the hole growth would be dominated by the fast rates of the centers near the laser frequency. At longer and longer times, the centers further from the laser produce a slower and slower hole growth rate.

Figure 18 shows a comparison of the predictions of Eq. (11) with the experimental hole growth data of Fig. 4. The integral was performed using Romberg and Gaussian methods,[15] and the fit shown has only two free parameters[16]: the pumping parameter amplitude P_0 and the

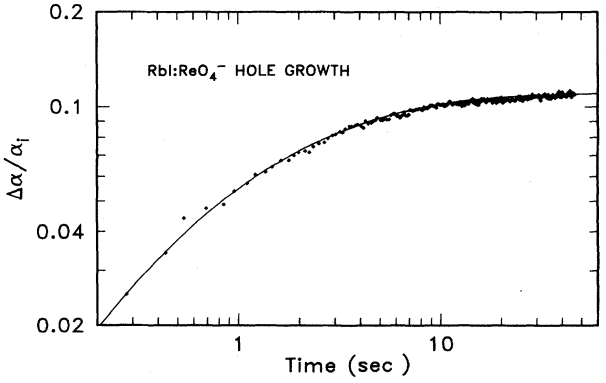

FIG. 18. Hole depth vs burning time for RbI:ReO_4^- at 1.2 K. The solid curve is the prediction of Eq. (11) for $P_0=12, \langle\Delta^2\rangle/\Gamma^2=0.89$. The points are the data of Fig. 4.

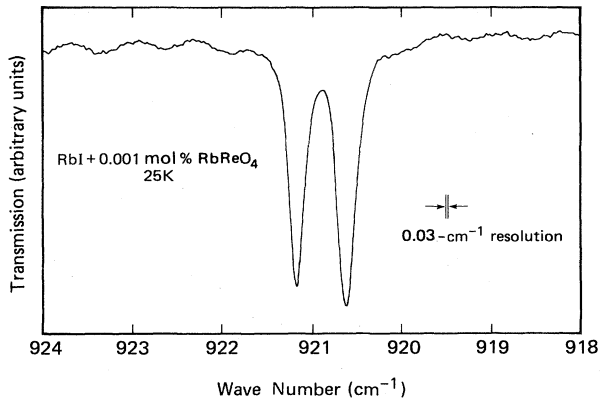

FIG. 19. Infrared transmission spectrum of RbI+0.001 mol % $RbReO_4$ at 25 K.

mean square splitting, $\langle\Delta^2\rangle$. (For calculational simplicity, all frequencies are measured in units of the homogeneous linewidth, hence Γ is set equal to 1.) The former parameter shifts the curve along the time axis and the latter parameter shifts the fit along the $\Delta\alpha/\alpha_i$ axis. The fit required $\langle\Delta^2\rangle/\Gamma^2=0.89\pm0.1$, which is consistent with the requirement that $\langle\Delta^2\rangle<\Gamma^2$. The required value of P_0 was 12 ± 1. Inspection of Eqs. (4) and (11) shows that the physical meaning of the product $P_0\Gamma$ is the probability of reorientation per center per second. Thus $P_0\Gamma$ may be written

$$P_0\Gamma=\mathcal{N}\mathcal{A}\eta\ , \tag{12}$$

where $\mathcal{N}$ is the number of photons per second, $\mathcal{A}$ is the absorption probability per center per photon, and where η is the quantum efficiency for reorientation per center per photon absorbed. Using the absorption cross section σ of Sec. III D, we immediately produce the simple relation

$$P_0=\frac{\sigma I}{\Gamma h\nu}\eta\ , \tag{13}$$

where I is the beam intensity, ν is the beam frequency, and h is Planck's constant. Thus the fit of Fig. 18 would yield a value of $\eta=6\times10^{-3}$, which differs by only a factor of 3 from the effective quantum efficiency η_e calculated in Sec. III D. Thus the photon-induced reorientation model describes the measured growth data of Fig. 18 reasonably well, although small departures of the model from the data are evident at large times and at small times.

The photon-induced reorientation model describes the steady-state and transient features of persistent hole burning for ReO_4^- molecules in alkali halides quite well. In particular, the predictions of this model are inconsistent with models of photochemical hole burning or with models in which the shift in transition frequency Δ is large compared with the homogeneous linewidth. Nevertheless, persistent nonphotochemical spectral holes (with somewhat different systematics) will result from any Δ distribution that is at least larger than the laser linewidth.

The success of this phenomenological photon-induced reorientation model is encouraging. It would be more satisfying, however, to find experimental evidence for a microscopic model like Fig. 16, where tunneling between librational levels of the vibrational ground state provides the mechanism for reorientation. Accordingly, to complement the extremely high-resolution limited-range (0.2–0.3 cm^{-1}) spectroscopy of Ref. 7, we have performed high-resolution (0.03 cm^{-1}) linear spectroscopy of the ν_3 mode vibrational absorption over a 6-cm^{-1} range. Figure 19 shows the resulting transmission spectrum of annealed RbI+0.001 mol % $RbReO_4$ taken at 25 K with a Fourier-transform infrared spectrometer. (Lower temperatures could not be reached with the cold-finger optical cryostat in use.) The strong doublet is due to the two isotopes of Re, and the baseline oscillations with 0.7-cm^{-1} period are due to Fabry-Perot resonances. Unfortunately, no strong librational sidebands are evident; librational sidebands, if present, must be weak. It remains for future experiments to elucidate the exact microscopic mechanisms responsible for the photon-induced reorientation.

V. CONCLUSION

Using a variety of CO_2-laser and diode laser spectroscopic techniques, the properties of persistent spectral holes in the vibrational-mode absorption of a spherical-top molecule embedded in a cubic site of alkali-halide lattices have been described and analyzed. The essential features of the phenomenon are well described by a photon-induced reorientation model. These results stand in sharp contrast to earlier nonphotochemical hole-burning studies in organic crystals and glasses. In particular, photophysical spectral hole formation can occur even though the host lattice undergoes no structural rearrangements or tautomerism. Persistent nonphotochemical hole burning is thus shown to be a general solid-state phenomenon which can occur whenever the complete ground state of the system has configurational degeneracy.

ACKNOWLEDGMENTS

The authors gratefully acknowledge the use of diode lasers from General Motors Research Laboratories, the use of a CO_2 laser from Professor David Lee of Cornell University, and the use of an IR-98 Fourier-transform infrared spectrometer from IBM Instruments. The assistance of David Lambert is also greatly appreciated. This work has been supported in part by U. S. Army Research Office Grant No. DAAG-29-79-C-0170, by National Science Foundation Grant No. DMR-80-08546, by National Science Foundation Grant No. DMR-79-24008 through the Cornell Materials Science Center, and by the U. S. Navy Office of Naval Research. The experimental data reported in this article were taken while one of the authors (W.E.M.) was located at Cornell University and while another author (A.R.C.) was located at General Motors Research Laboratories.

[1]J. M. Hayes, R. P. Stout, and G. J. Small, J. Chem. Phys. 74, 4266 (1981).

[2]F. G. Patterson, H. W. H. Lee, R. W. Olson, and M. D. Fayer, Chem. Phys. Lett. 84, 59 (1981).

[3]M. Dubs and H. H. Günthard, Chem. Phys. Lett. 64, 105 (1979).

[4]A recent review of photochemical hole burning may be found in L. A. Rebane, A. A. Gorokhovskii, and J. V. Kikas, Appl. Phys. B 29, 235 (1982).

[5]W. E. Moerner, A. J. Sievers, R. H. Silsbee, A. R. Chraplyvy, and D. K. Lambert, Phys. Rev. Lett. 49, 398 (1982).

[6]W. E. Moerner, Ph.D. thesis, Cornell University, 1982 (unpublished); Cornell Materials Science Center Report No. 4588 (unpublished).

[7]A. R. Chraplyvy, W. E. Moerner, and A. J. Sievers, Opt. Lett. 6, 254 (1981).

[8]A. R. Chraplyvy, W. E. Moerner, and A. J. Sievers, Opt. Lett. 6, 431 (1981); W. E. Moerner, A. J. Sievers, and A. R. Chraplyvy, Phys. Rev. Lett. 47, 1082 (1981); W. E. Moerner, A. R. Chraplyvy, and A. J. Sievers (unpublished).

[9]A. J. Sievers, Phys. Rev. Lett. 13, 310 (1964).

[10]R. M. Macfarlane, R. M. Shelby, A. Z. Genack, and D. A. Weitz, Opt. Lett. 5, 462 (1980).

[11]Frank Bridges, private communication and unpublished results.

[12]M. R. Mohammad and W. F. Sherman, J. Phys. C 14, 283 (1981).

[13]W. D. Seward and V. Narayanamurti, Phys. Rev. 148, 463 (1966).

[14]S. J. Hunter, K. W. Hipps, R. Bramley, and A. H. Francis, Chem. Phys. 45, 149 (1980).

[15]A. Ralston and P. Rabinowitz, *A First Course in Numerical Analysis,* 2nd ed. (McGraw-Hill, New York, 1978).

[16]This statement must be qualified slightly in the following sense. The experimental value of T_i cannot be measured exactly due to time constant limitations; however, T_i can be determined to 10—15 % relative accuracy. The value of T_i used to compute $\Delta\alpha/\alpha_i$ changes the shape of the experimental curve in Fig. 18 at short burning times. To improve the fit, T_i was varied over a 5—10 % range, well within the allowed actual values, hence T_i is not a free parameter.